Pancreatic α and β cells are globally phase-locked

Huixia Ren[1,2,3,5], Yanjun Li[1,5], Chengsheng Han[2,5], Yi Yu[1], Bowen Shi[3], Xiaohong Peng[2], Shufang Wu[1], Wenzhen Zhu[2], Guoyi Yang[2], Xiaojing Yang[1,3], Kim Sneppen[4], Liangyi Chen[2*], and Chao Tang[1,3*]

[1]Center for Quantitative Biology, Peking University, Beijing 100871, China
[2]Institute of Molecular Medicine, Peking University, Beijing 100871, China
[3]Peking-Tsinghua Center for Life Sciences, Peking University, Beijing 100871, China
[4]Niels Bohr Institute, University of Copenhagen, 2100 Copenhagen, Denmark
[5]Equal Contribution
*Correspondence: lychen@pku.edu.cn; tangc@pku.edu.cn

ABSTRACT

The Ca^{2+} modulated pulsatile secretions of glucagon and insulin by pancreatic α and β cells play a key role in glucose metabolism and homeostasis. However, how different types of islet cells couple and coordinate via paracrine interactions to produce various Ca^{2+} oscillation patterns are still elusive. By designing a microfluidic device to facilitate long-term recording of islet Ca^{2+} activity at single cell level and simultaneously identifying different cell types in live islet imaging, we show heterogeneous but intrinsic Ca^{2+} oscillation patterns of islets upon glucose stimulation. The α and β cells oscillate in antiphase and are globally phase locked to various phase delays, causing fast, slow or mixed oscillations. A mathematical model of coupled phase oscillators quantitatively agrees with experiments and reveals the essential role of paracrine regulations in tuning the oscillation modes. Our study highlights the importance of cell-cell interactions to generate stable but tunable islet oscillation patterns.

Keywords: Islet, Ca^{2+} oscillation, β cell, α cell, paracrine regulation, spatial-temporal analysis, synchronization, phase locking, mathematical modeling

Introduction

To precisely regulate the blood glucose level[1–3], glucose elevation induces Ca^{2+} oscillations in pancreatic islet cells that triggers pulsatile secretions of insulin and glucagon[4–7]. Dampening and disappearance of islet Ca^{2+} oscillation is an early biomarker in the pathogenesis of type 2 diabetes[8–11]. Multiple types of oscillation patterns have been observed in islets, including fast (~10s cycle), slow (~100s cycle), and mixed oscillations (10 ~100s cycle)[12–14]. While different mathematical models have been proposed to explain the underlying mechanism[15–18], most regarded Ca^{2+} oscillation as determined by the intrinsic properties of single β cells, such as endoplasmic reticulum Ca^{2+} buffering capacity[18] and the slow metabolic cycle of ATP/ADP ratio during glucose stimulation[17]. These single-cell models, however, cannot explain the observed variety of oscillation patterns - only slow Ca^{2+} oscillations are seen in isolated β cells[19–22]. In islets, α and β cells show highly correlated Ca^{2+} oscillation patterns[23], while periodical releases of insulin and glucagon are also temporally coupled both *in vitro*[4,24] and *in vivo*[6,7,25,26]. Given the extensive autocrine and paracrine interactions between α and β cells[27–32], they may critically modulate or even dictate the islet oscillation modes.

The ultimate challenge to test such a hypothesis lies in the ability to resolve the identities of individual cells and to simultaneously monitor their activity in live islets. In addition, because the spatial organizations of α and β cells are highly heterogeneous from islet to islet[33,34], quantitatively comparing Ca^{2+} oscillations in different islets is difficult. To address this problem, we have developed a microfluidic device attached to the spinning-disc confocal microscope, which allows individual cells to be imaged under physiological conditions for up to ~2 hrs. By long-term imaging of islets undergone repeated glucose stimulation, we showed that oscillation mode represents the intrinsic property of the islet. Quantitative analysis revealed generic features and quantitative relationship in these oscillation patterns. With genetic labelling that distinguishes the Ca^{2+} activities between α and β cells, we found synchronized anti-phase Ca^{2+} oscillations between islet α and β cells, in which different phase delays conferred different oscillation modes. Finally, we developed a coarse-grained mathematical model that captures the paracrine interactions between α and β cells. The model reproduced key quantitative features of the experimentally observed oscillations, and predicted that different oscillation modes are results of varied paracrine controls.

Results

Glucose-Evoked Ca^{2+} Oscillation Represents an Intrinsic Property of the Islet

To provide a stable and controllable environment for long-term imaging of intact islet, we developed a microfluidic device (Fig. 1a). On one side, we designed an inlet port for the loading of islets (300 μm in width and 270 μm in height), which could be sealed after the loading. The chip was able to trap islets of different size with a descending PDMS ceiling (270, 180, 150, 110, 80 and 50 μm in height). Meanwhile, the solution bypassing the islet could be collected for hormone detection at the outlet port. On the side opposite to the inlet, five independent input channels merged into one channel upstream of the islet trapping site. Such a device enabled long-term and stable imaging of islets even during the switching of different perfusion solutions. For instance, when glucose concentration in the perfusion solution was increased from 3 to 10 mM (3G to 10G), all islets exhibited an initial rapid rise in cytosolic Ca^{2+}, followed by the gradual appearance of fast (a cycle < 60 s, 31 of 46 islets), slow (a cycle > 60 s, 9 of 46 islets) or mixed (6 of 46 islets) Ca^{2+} oscillations (Figs. 1b and 1c). In contrast, although high glucose still evoked the initial increase in cytosolic Ca^{2+} concentration, no following periodic Ca^{2+} oscillations were observed in isolated islets from diabetic *db/db* mice (9 of 9 islets, Fig. 1b lower panel)[10,11], reinforcing the critical role of Ca^{2+} oscillation in maintaining normal hormone release and glucose homeostasis. While different islets displayed largely variable Ca^{2+} oscillations, a second round of 10G stimulation in the same islet evoked an oscillation frequency nearly identical to that of the first round (Figs. 1b and 1c). The spatial activation profiles between two rounds of stimulation were also similar. Nearly identical cells lighted up at the designated times of Ca^{2+} cycles during the two rounds of stimulation (Fig. 1d and Extended Data Fig. 1, Video 1-2). which was quantified by the fact that sequential activations of islet cells between two rounds of stimulations showed significantly higher similarity indexes than random associations (Fig. 1e and Extended Data Fig. 2, See Methods). Therefore, specific oscillation modes represent a robust intrinsic property of individual islets, possibly determined by the fixed spatial organization of the islet.

Islet α and β Cells Are Globally Phase-Locked

To probe the specific micro-organization of an islet and to distinguish the Ca^{2+} activities between α and β cells, we need to resolve different types of islet cells. We thus generated *Glu-GCaMP6f Ins2-RCaMP1.07* mice, in which α cells expressed green fluorescent Ca^{2+} sensor GCaMP6f and β cells red fluorescent Ca^{2+} sensor RCaMP1.07 (see Methods) (Figs. 2a and 2b).

By simultaneous imaging the α and β cell Ca^{2+} activities from 21 dual-color Ca^{2+}-labeled islets, we were able to observe altogether the activities of 819 α cells and 166 β cells. Interestingly, although α cells in the islet exhibited variable Ca^{2+} transients in resting glucose concentration, they became highly synchronized during 10G stimulation (Figs. 2c and 2d, Video 3). Unlike β cells that are inter-connected by the gap junction protein connexin 36 to achieve synchronization[35–38], α cells do not express gap junction proteins and are thus not physically connected to each other[39]. We observed that the mean Ca^{2+} peaks of α cells displayed a fixed delay to those of β cells, suggesting that the highly synchronous α cell activity was due to stable phase-locking to the β cell activity (Figs. 2e and 2f). Consistent with α cells being tightly regulated by paracrine inhibition originating from their

neighboring β cells, we observed global α cell activation after the turning-off of β cells (Fig. 2g). Intriguingly, phase-locking with the similar temporal characteristics was also present in slow and mixed oscillations (Fig. 2h, Video 4-5), suggesting a common underlying mechanism. Taken together, these data demonstrated that α cells are stably, globally and universally phase-locked to β cells under elevated glucose stimulation.

Variable Delay of β Cell Activation After α Cell Determines the Oscillation Mode

To non-biasedly sort out critical parameters differentiating various Ca^{2+} oscillation patterns, we quantitatively defined features of each oscillation cycle of alternately activated α and β cells (Fig. 3a). The oscillation period T was defined as the time window between one cycle of β cell activation, which was split into two parts: the waiting time for α cells to activate after β cell activation ($T_{\beta\alpha}$), and the waiting time for β cells to activate after α cell activation ($T_{\alpha\beta}$). The phase difference ($\Delta\theta$) of two types of cells was defined as the ratio between $T_{\beta\alpha}$ and T. There were multiple ways to define these quantities – either using peak, 25%, 50%, or 75% decrease - and they did not change the outcome of the analysis (Extended Data Fig. 4). In addition, we also defined other features that recapitulated different characteristics of the α and β cell Ca^{2+} dynamics, such as the rise and decay time of the activation for α and β cells, the Full Width at Half Maximum (FWHM), etc. In total, each oscillating cycle was vectorized into 13 features (see Extended Data Fig. 3 and Supplementary Information for detailed definitions), which were assembled into a feature matrix. Next, by dimension reduction of these parameters with the UMAP algorithm [40], the oscillations could be classified into the fast and the slow ones (Fig. 3b), in which T, $\Delta\theta$, $T_{\alpha\beta}$ and FWHM of β cells demonstrated significant inter-group differences (Fig. 3c and Extended Data Fig. 5). The T for the fast oscillations centered at ~30 s, much faster than that of the slow oscillations (~100 s). The average $\Delta\theta$ for the fast oscillation cycles was ~0.7, compared to ~ 0.2 for the slow ones. Mean $T_{\alpha\beta}$ for the fast oscillations was smaller than that for the slow oscillations (~10 s versus ~81 s, Table 1). The distribution of FWHM of fast Ca^{2+} oscillations of β cells was different from that of the slow ones, with a mean FWHM at ~11 s for the fast oscillations versus ~31 s for the slow oscillations (Table 1). In contrast, the distributions of the waiting time $T_{\beta\alpha}$ and the rise time of α cell activation τ_{α_up} were indistinguishable between the fast and the slow oscillations (~20 s and 5 s, respectively, Fig. 3c), while the distributions of FWHM for α cell Ca^{2+} were also similar between fast and slow oscillations. Note that this would imply a higher FWHM ratio of the Ca^{2+} transients of α to β cells in fast Ca^{2+} oscillations (~1) than in the slow oscillations (~0.5) (Extended Data Fig. 5).

As T, $\Delta\theta$, $T_{\alpha\beta}$ and $T_{\beta\alpha}$ were inter-dependent parameters, we further evaluated their relationship using scatter plots (Fig. 3d). It was apparent that $T_{\beta\alpha}$ remained constant across different T. In contrast, $\Delta\theta$ was inversely proportional to T, and $T_{\alpha\beta}$ increased linearly with T. These findings strongly suggest a key role of $T_{\alpha\beta}$ in determining the period (hence the mode) of β cell Ca^{2+} oscillation. While a short

waiting time $T_{\alpha\beta}$ leads to fast oscillation, long waiting time $T_{\alpha\beta}$ confers slow oscillation. Because isolated single β cells displayed only slow oscillation with a period of about 5 minutes (Extended Data Fig. 6), we speculate that increased stimulatory effect from α cells to β cells may push β cells to oscillate in the fast mode.

Interestingly, sometimes we observed spontaneous switching of β cells from the fast to the slow oscillations within the same islet, accompanied by a prolonged delay of β cell activation after α cell activation (Fig. 3e). This data corroborated our analysis conducted in multiple islets, and also pointed to the possibility of dynamic changes in the interactions between α and β cells in the same islet.

Mathematical Modeling

We observed that islets show heterogenous yet intrinsic oscillation patterns under high glucose stimulation. To better understand the origin of various oscillation modes and the factors controlling them, we developed a mathematical model incorporating interactions between α and β cells.

α-β Phase Oscillator Model

Given the fact that both α cells and the β cells in an islet were globally synchronized respectively, we simplified the islet as a model of two coupled "cells" - an α cell and a β cell (Fig. 4a). The oscillation of each cell was described by a phase variable θ, which was driven by an intrinsic force as well as a paracrine force (Fig. 4b, see Supplementary Information). The intrinsic term corresponded to the oscillation frequency of the isolated single cells. As previous studies and our own studies have shown, single β cells oscillate with a period around 3-5 minutes and single α cells oscillate with a period around 30-60 seconds (Extended Data Fig. 6). The paracrine term consisted of three parts: $f_s(\theta)$ represented the hormone secretion, $f_{r\alpha}(\theta)$ represented the paracrine inhibition of α cells by β cells, and $f_{r\beta}(\theta)$ represented the paracrine stimulation of β cells by α cells. The main results of the model were insensitive to the choice of specific forms of $f_s(\theta)$, $f_{r\alpha}(\theta)$ and $f_{r\beta}(\theta)$ as long as they were periodic functions resembling the general characteristic of the biology (see Extended Data Figs. 7 and 8 for details). The coefficients $K_{\alpha\beta}$ and $K_{\beta\alpha}$ represented the coupling strengths between the α and β cells. Note that this is a two-phase model without providing any information on the amplitude of the oscillation. Its behavior can be characterized by the "winding number" defined as the asymptotic ratio of the two phases $w = \theta_\alpha/\theta_\beta$ (Fig. 4c).

Slow, Fast and Mixed Oscillations

By adjusting the coupling strengths ($K_{\alpha\beta}$ and $K_{\beta\alpha}$) between the α and β cells, our model displayed all three types of the oscillation behaviors observed in experiments (cases 1-3, Fig. 4d). When α cell weakly stimulated β cell (small $K_{\alpha\beta}$), the model islet generally showed slow oscillations. When α cell and β cell were strongly coupled with each other (large $K_{\beta\alpha}$ and $K_{\alpha\beta}$), the model islet generally showed

fast oscillations. When α cell strongly stimulated β cell and β cell weakly inhibited α cell (large $K_{\alpha\beta}$ and small $K_{\beta\alpha}$), the model islet generally showed mixed oscillations. With very weak coupling between the α and β cells, the model displayed an oscillation behavior similar to uncoupled single cells but not islet experiments (Fig. 4d, case 4). Further quantification found the phase difference $\Delta\theta$ and the period T (see Fig. 3a for definition) displayed an inverse proportional relationship (Fig. 4f, left panel), which was because of a constant waiting time of the α cell regardless of the oscillation modes (Fig. 4f, middle panel), similar to experimental data (Fig. 3e). The coupling coefficients changed only the waiting time of the β cell, and further determined the period (Fig. 4f, right panel).

Phase Locking Between α and β Cells

We next analyzed the behavior of the model by systematically varying the coupling strengths between the α and β cells. We found that the α and β cells were generally phase locked, i.e. their phases were dependent on each other with a fixed relationship characterized by the winding number w (Fig. 4c). By plotting the dependence of the winding number on the coupling strengths, we obtained the phase space of the system of two coupled oscillators (Fig. 4e). It formed a structure of two-dimensional Arnold tongues[41], which could be separated in four regions (Fig. 4e, see Supplementary Information). In region 1, the α cell and the β cell are locked on the w=1/1 mode. That is, when θ_β finishes one cycle ([0,2π]), θ_α will also finish one cycle. An example of this oscillation mode is shown in Fig. 4d (upper panel). In region 2, the two cells are locked in the mode w=0/1. That is, when θ_β finishes one cycle ([0,2π]), θ_α cannot finish a full cycle before being pushed back (Fig. 4d, middle upper panel). In region 3, the two cells are locked with w<1. In particular, there exist w=m/n modes, where m<n are both integers. In a mode with w=m/n, when θ_β finishes n cycles ([0,2$n\pi$]), θ_α will finish m cycle(s) ([0, 2$m\pi$]). An example with w=1/2 is shown in Fig. 4d (middle lower panel). As can be seen from the figure, while each activation of the β cell can finish one full cycle, the first activation of α cell cannot finish a full cycle before being pushed back, and only the second activation can finish a full cycle. Although only a few modes are shown in region 3 for clarity, it can be proved rigorously that region 3 contains all the modes with w being a rational number between 0 and 1 (unpublished). In region 4, the two phases are locked with w>1, which means that α cell will finish more cycles than β cell. An example of w=3/1 is shown in Fig. 4d (lower panel). In this region, α and β cells couple weakly. At the corner $K_{\alpha\beta}$=$K_{\beta\alpha}$=0, α and β cells completely decouple and beat on their own frequencies. Note that while w jumps discontinuously with continuously varying parameters, the average period of β cell oscillation changes smoothly (Fig. 4e, heat map). Thus, the paracrine interactions between α and β cells offer robust and tunable oscillation patterns and periods.

Model Prediction and Verification

A prediction of the model was that the oscillation period may be tuned with the strengths of paracrine interaction. In particular, increasing the activation from α cell to β cell ($K_{\alpha\beta}$) would decrease the oscillation period, especially in islets of slow oscillations (Fig. 4e, heat map). To test this prediction, we applied glucagon (100 nM) to the islets showing fast and slow oscillations (Fig. 5a). While adding glucagon hardly affected the fast oscillating islets, it switched the slow oscillating islets to fast

oscillations (Figs. 5a, 5b and Extended Data Fig. 9). According to our model, the change of oscillation period was due to the reduction of the waiting time $T_{\alpha\beta}$ without affecting the waiting time $T_{\beta\alpha}$. Experimental data faithfully recapitulated this prediction (Figs. 5c, 5d and Extended Data Fig. 9). Therefore, more glucagon actions correspond to stronger paracrine interactions, shorter $T_{\alpha\beta}$ and fast oscillation; in contrast, less glucagon actions lead to more autonomous cellular regulation and slow oscillations. In addition, our model also predicted that in mixed oscillation mode, decay times of Ca^{2+} transients in α cells were different - only the last Ca^{2+} transient in each cluster of cycles of mixed oscillation was independent of β cells, while all other ones were repressed by β cells and should descend faster (Fig. 5e). By analyzing the Ca^{2+} traces of islets with mixed oscillation modes, we confirmed that the decay times of α cell transients fell into two groups: the Ca^{2+} transients in α cells just preceding an uprising of β cell activation decayed faster, while the ones posterior to β cell transients exhibited a significantly slower decay (Fig. 5f and Extended Data Fig. 10). This highlights the importance of α-β interactions in shaping up the oscillation modes (see Supplementary Information).

Discussion

In this study, we developed a microfluidic device that enabled stable and repeatable long-term imaging of Ca^{2+} activities of islets at single cell resolution. Despite the apparent heterogeneity in Ca^{2+} activities across different islets, individual islets exhibited their own spatial and temporal patterns of Ca^{2+} oscillations that were repeatable under multiple rounds of glucose stimulation. This suggests that the oscillation mode is a result of some intrinsic property of the islet, possibly correlated with different cell types and their spatial distributions within the islet.

By using the *Glu-GCaMP6f Ins2-RCaMP1.07* transgenetic mice, we discovered that the α and β cells were globally phase locked to various oscillation modes. Besides α and β cells, δ cells have received increasing attentions in glucose regulation recently[42], but are not included in the current model. δ cells are connected to β cells by gap junctions and exhibit Ca^{2+} activities similar to β cells [43]. Therefore, the group containing β cells would presumably also have δ cells in it (unpublished). In our mathematical model of this study, the role of δ cells in regulating the oscillation modes was lump summed together with that of β cells. Obviously, it is important to differentiate the two types of cells in future modeling.

A key finding in our study is that the time delay for α cells' activation following the activation of β cells ($T_{\beta\alpha}$) was invariant, regardless of the islet-to-islet variations in oscillation frequencies and modes. This interesting observation echoed nicely with the ~20 seconds recovery time of α cells from the relief of optogenetic activation of β cells[43]. Therefore, $T_{\beta\alpha}$ is likely to be determined by the temporal relief of α

cells from the inhibition by β cells through δ cells, which is a constant independent of experimental condition. In contrast, what varied in different islets under different conditions was the time delay of β cells' activation following that of α cells ($T_{\alpha\beta}$), which sets the frequency and mode of the oscillation. All these features were accurately recaptured quantitatively by our mathematical model.

In our study, both experimental observations and model simulations showed robust phase locking phenomenon between α and β cells. It is known that faster islet Ca^{2+} oscillations display more regular oscillation patterns[13,44]. In light of our findings, the increased regularity may come from the increased stability in phase locking: a faster oscillation implies a stronger activation from α to β cells and thus a tighter phase locking. The Ca^{2+} oscillation of the two types of cells can phase lock to a variety of modes, determined by the paracrine interactions, which not only have different oscillation frequencies, but also display a range of other quantitative features such as the winding number and the ratio of the half-widths for α and β transients. Phase-locking to different frequencies and modes could ensure a stable and tunable secretion of insulin and glucagon, not only for their amounts, but also for their ratio. Different modes of β cell Ca^{2+} oscillations were observed *in vivo*, including those of fast ones[45–47]. Further studies combining islet Ca^{2+} imaging with real-time detection of α and β cell secretion are needed to investigate the physiological roles of the phase locking and its dependency on paracrine interactions.

Methods

Animal studies

Glu-Cre mice were isolated from the *GluCre-Rosa26*^{EYFP} (GYY) mice provided by Herbert Y. Gaisano Lab of the University of Toronto (Toronto, Canada). *Lck-GCaMP6f*^{flox} mice were obtained from Jackson Laboratory (stock number 029626, 003314). *Glu-GCaMP6f* mice were generated by crossbreeding *Glu-Cre* mice with *Lck-GCaMP6f*^{flox} mice. To generate *Ins2-RCaMP1.07* mice, the targeting vector was constructed with *Ins2* 5'promoter, *RCaMP1.07* and *Ins2* 3'fragment as described in Fig. 2c. The vector was then injected with PiggyBac mRNA to the zygotes of C57BL/6J mice (conducted by the Model Animal Research Center of Nanjing University, Nanjing, China). The vector was randomly inserted to the genome using the PiggyBac transposons system and the β cells were sparsely labeled with RCaMP1.07. By crossbreeding *Ins2-RCaMP1.07* mice with *Glu-GCaMP6f* mice, both α and β cells were labeled by different fluorescent Ca^{2+} indicators. All mice were genotyped by PCR using template tail DNA extracted by the TIANamp Genomic DNAKit (DP304, TIANGEN). *Ins2-RCaMP1.07* mice were PCR genotyped with PrimeSTAR® GXL DNA Polymerase (R050A, Takara) using primers (forward 5'-TGTTTCCGGTCTGACTCTGATTCC-3', reverse 5'-GACCGGCCTTATTCCACTTACGAC-3'). Other mice were PCR genotyped with 2x EasyTaq® PCR SuperMix (AS111, TRANSGEN). Genotyping primers and protocols have been reported previously[1] or are available online (https://www.jax.org/strain/029626). *Leprdb/Leprdb (db/db)* and age-matched C57BL/6J mice (male) were purchased from the Model Animal Research Center of Nanjing University, Nanjing, China. Mice were maintained in one cage with a light/dark cycle of 12 h and administered chow diet ad libitum. Only male mice aged 8-20 weeks were used in the study. All animal experiments were conducted in accordance with the institutional guidelines for experimental animals at Peking University, which were approved by the AAALAC.

Design and application of microfluidic chip

For the microfluidic chip, PDMS was used as the channeled substrate, and glass coverslips (24 x 60 mm) were used as the floor substrate, as shown in detail in Fig. 1a. We used the photo-polymerizable epoxy resin (SU-8-2100) to make a positive relief master, and the PDMS substrate was cured on the master. The islet trapping region was designed as a stair-like channel, using six different thicknesses of SU-8 photoresist. To trap islets of different sizes, the heights of this region were designed to be 50, 80, 110, 150, 180, 270 μm. Solution passing through the islet could be collected at the outlet region. The microfluidic chip was pre-filled with KRBB solution (125 mM NaCl, 5.9 mM KCl, 2.56 mM $CaCl_2$, 1.2 mM $MgCl_2$, 1 mM L-glutamate, 25 mM HEPES, 0.1% BSA, pH 7.4) containing 3 mM D-glucose before use. To achieve a stable hour-long imaging, we degassed the liquid. We injected the islet into the microfluidic chip by using a 10μL pipette.

Isolation and culture of mouse pancreatic islets

Pancreatic islets were isolated from mice as previously described[2]. Then they were cultured in RPMI 1640 medium (11879020, Gibco) supplemented with 10% fetal bovine serum (10099141C, Gibco),

5.5 mM D-glucose, 100 unit/ml penicillin and 100 g/ml streptomycin. They were maintained at 37℃ and 5% CO_2 in a culture incubator before the imaging experiments.

Dissociation into single-cells

After overnight culturing, the isolated islets were washed with HBSS (14175095, Gibco). They were then digested with 0.25% trypsin-EDTA (25300-062, Gibco) for 3 min at 37℃ followed by a brief shaking. The digestion was stopped by the culture medium, and centrifuged at 1000 rpm for 5 min. The cells were suspended by RPMI 1640 culture medium. The cell suspension was plated on coverslips in the poly-L-lysine-coated Glass Bottom Dish (D35-14-1-N, Cellvis) or the microfluidic chip. The dishes or chips were then kept for 40 min in the culture incubator at 37℃, 5% CO_2 to allow cells to adhere. Additional culture medium was then added, and the cells were cultured for 24 h before the imaging experiments.

Fluorescence imaging of Ca^{2+}

For samples isolated from C57BL/6J or *db/db* mice, we loaded the samples with Cal-520 AM dye (2 μM, 37℃, 40 min) for Ca^{2+} imaging experiments. For samples isolated from *Glu-GCaMP6f Ins2-RCaMP1.07* mice, we directly imaged GCaMP6f and RCaMP1.07 signals. In our experiments, we used two confocal spinning-disc microscopes and one two-photon microscope. One of the confocal microscopes is an inverted TiE microscope (Nikon) attached to an UltraVIEW VOX system spinning disc (PerkinElmer) with a C9100-13 EMCCD camera (Hamamatsu), which was controlled by the Volocity software (PerkinElmer) and equipped with a 40×/1.25 NA objective (Nikon CFI APO). For 2% transmission of 561 nm illumination (50 mW) and 20% transmission of 488 nm illumination (40 mW), the exposure was set to 20 ms and 100 ms, respectively. The other confocal microscope was a Dragonfly 200 series (Andor) with a Zyla4.2 sCMOS camera (Andor), and the Fusion software. All channels were collected with a 40x/0.85 NA Microscope Objective (Warranty Leica HCX PL APO). For 1% transmission of 561 nm illumination (50 mW) and 3% transmission of 488 nm illumination (50 mW), the exposure was set to 20 ms and 100 ms, respectively. The islet in the microfluidic chip was kept in 37℃ and 5% CO2 on the microscope stage during imaging. The reagents were automatically pumped into the microfluidic chip with a flow rate of 400 μL/h by the TS-1B syringe pump (LongerPump), which was controlled by software written in MATLAB. The two-photon microscope equipped with one 40×/0.8 NA water Objective was used in previous works, detailed elsewhere[3].

Similarity index

The similarity index (SI) was defined to compare the spatial activation similarity between two rounds of 10G stimulation (3 seconds sampling interval). Firstly, we took 10-min images from the first round (R_1') and second round (R_2') respectively. Next, we used differences between two consecutive frames from the stacks R_1' and R_2' to form new stacks of R_1, R_2 which best highlighted the times and cells of large increases of fluorescence intensities. We selected individual Ca^{2+} transient sub-stacks of R_1,

R_2, and denoted them as $R_{1\text{-}1}$, $R_{1\text{-}2}$, ... and $R_{2\text{-}1}$, $R_{2\text{-}2}$…., where which $R_{1\text{-}i}$ was temporally aligned with $R_{2\text{-}j}$ according to peak times of Ca^{2+} transients (Extended Data Fig. 2a). We removed the last frames in cases when the original frames of $R_{1\text{-}i}$ and $R_{2\text{-}j}$ were not equal. Thus, the processed $R_{1\text{-}i}$ and $R_{2\text{-}j}$ had *t* frames.

The similarity index was used to define how similar two rounds of stimulations evoked responses from the same location. For a given pair of $R_{1\text{-}i}$, $R_{2\text{-}j}$, we selected a fixed region of interest of 150 pixels × 150 pixels (45 μm× 45 μm), and made montages which are indicated by the Target (*T*) and Paired (*P*) images for cross-correlations calculation (the size of the *T*, and *P* were 150*150*t*). We also randomly selected 50 regions of 150 pixels × 150 pixels in the $R_{2\text{-}j}$ sub-stack and indicated them as Random (R) to calculate the random similarity indexes (Extended Data Fig. 2a).

The image similarity was calculated by the pixel-based SSIM index [4]. The SSIM index of *T* and *P* was indicated by *SSIM*(*T*,*P*), and the mean SSIM index between *T* and *R* was indicated by $\overline{SSIM(T,R)}$. Because the perfect match conferred a SSIM index of 1, we defined the similarity index between *T* and *P* as the normalized SSIM index:

$$SI(T,P) = \frac{SSIM(T,P) - \overline{SSIM(T,R)}}{1 - \overline{SSIM(T,R)}}$$

According to the definition, a similar pair of *T* and *P* gives large *SI(T, P)*. When *T* and *P* were from the identical position from two rounds of 10G stimulation, *SI(T, P)* belonged to the "round1, 2 pair" category shown in Fig. 1e and Extended Data Fig. 2b. Otherwise *SI(T, P)* belonged to the "random pair" category shown in Fig. 1e and Extended Data Fig. 2b.

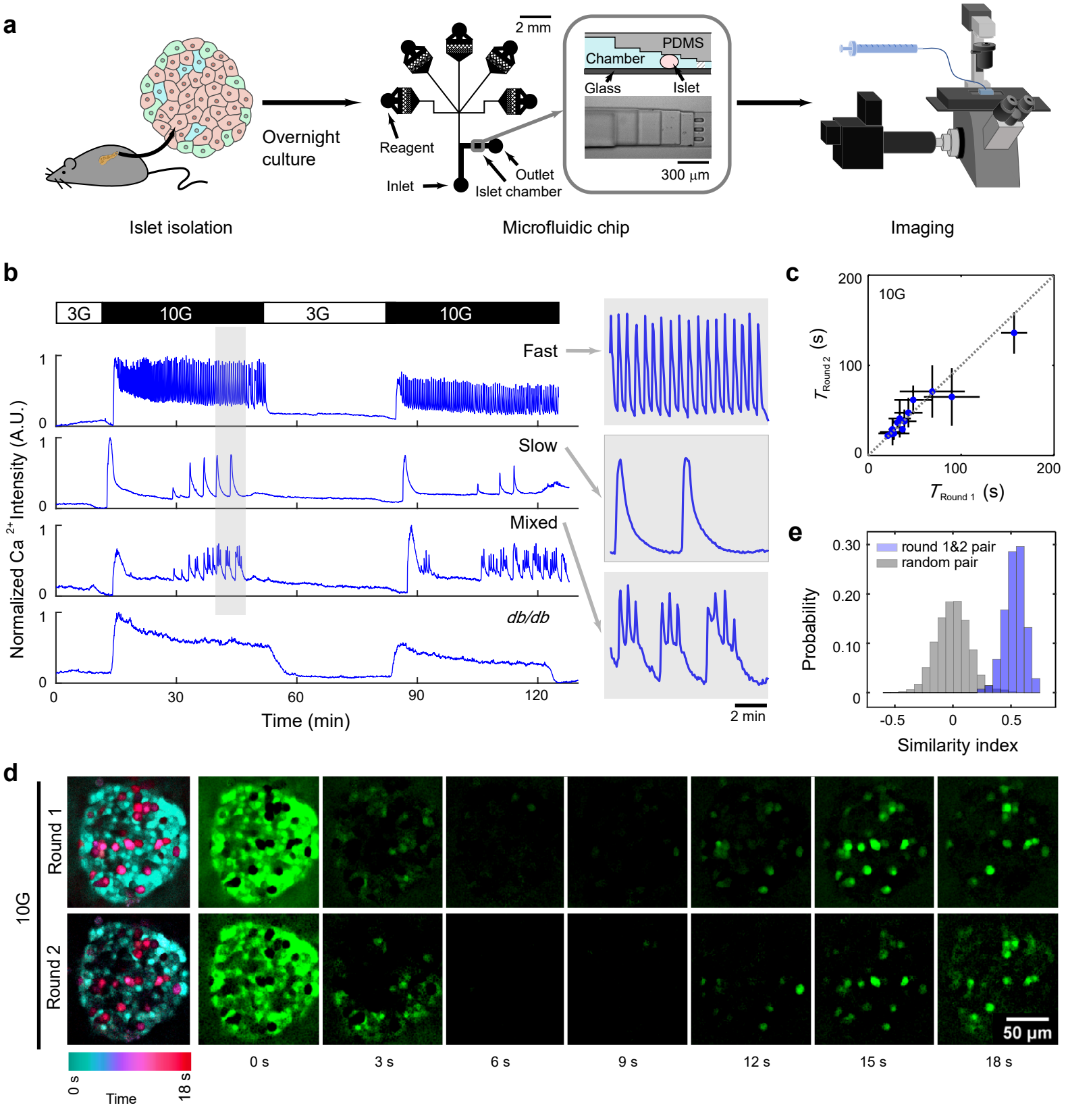

Fig. 1 | Islets show intrinsic Ca^{2+} oscillation modes under high glucose stimulation

Fig. 1 | Islets show intrinsic Ca^{2+} oscillation modes under high glucose stimulation

a, Experimental flow chart. Islets are isolated from mice. After overnight culture, the islets are loaded onto the microfluidic chip for imaging with confocal microscopy. The chip comprises five reagent channels, an inlet channel and an outlet channel. The islet chamber traps the islet with a gradient height from 270 μm to 50 μm. **b**, Representative recordings of whole islet Ca^{2+} signal in Cal-520-loaded islets isolated from C57BL/6J mouse. The islet is stimulated with a repeated protocol: 10 min 3 mM glucose (3G), 40 min 10 mM glucose (10G), 30 min 3G and 40 min 10G. First panel, islet displays fast oscillation with a period of ~20 s (31 of 46 islets); second panel, slow oscillation at ~3.5 min (9 of 46 islets); third panel, mixed oscillation at ~20 s and 2.45 min (6 of 46 islets); fourth panel, absence of Ca^{2+} oscillation in a *db/db* mouse islet (9 of 9 islets). Except for the last one, enlarged images of the shaded region are shown on the right. **c**, The mean Ca^{2+} oscillation period during the first *versus* the second round of 10G stimulation (n = 24 islets). **d**, Cell activation sequence in first and second round of 10G stimulation. We subtract the previous frame from the next frame of the original Ca^{2+} images (frame interval 3 s). Shown is the cell activation sequence averaged across oscillation cycles in a 5 min interval (aligned with the maximum activation frame) (Extended Data Fig. 1). Left panels summarize the time sequence shown in the 7 right panels, with the pseudo-color representing the activation time. **e**, The same islet shows high similarity index between the first and the second round of 10G stimulation (n = 5 islets) (see Methods and Extended Data Fig. 2 for details).

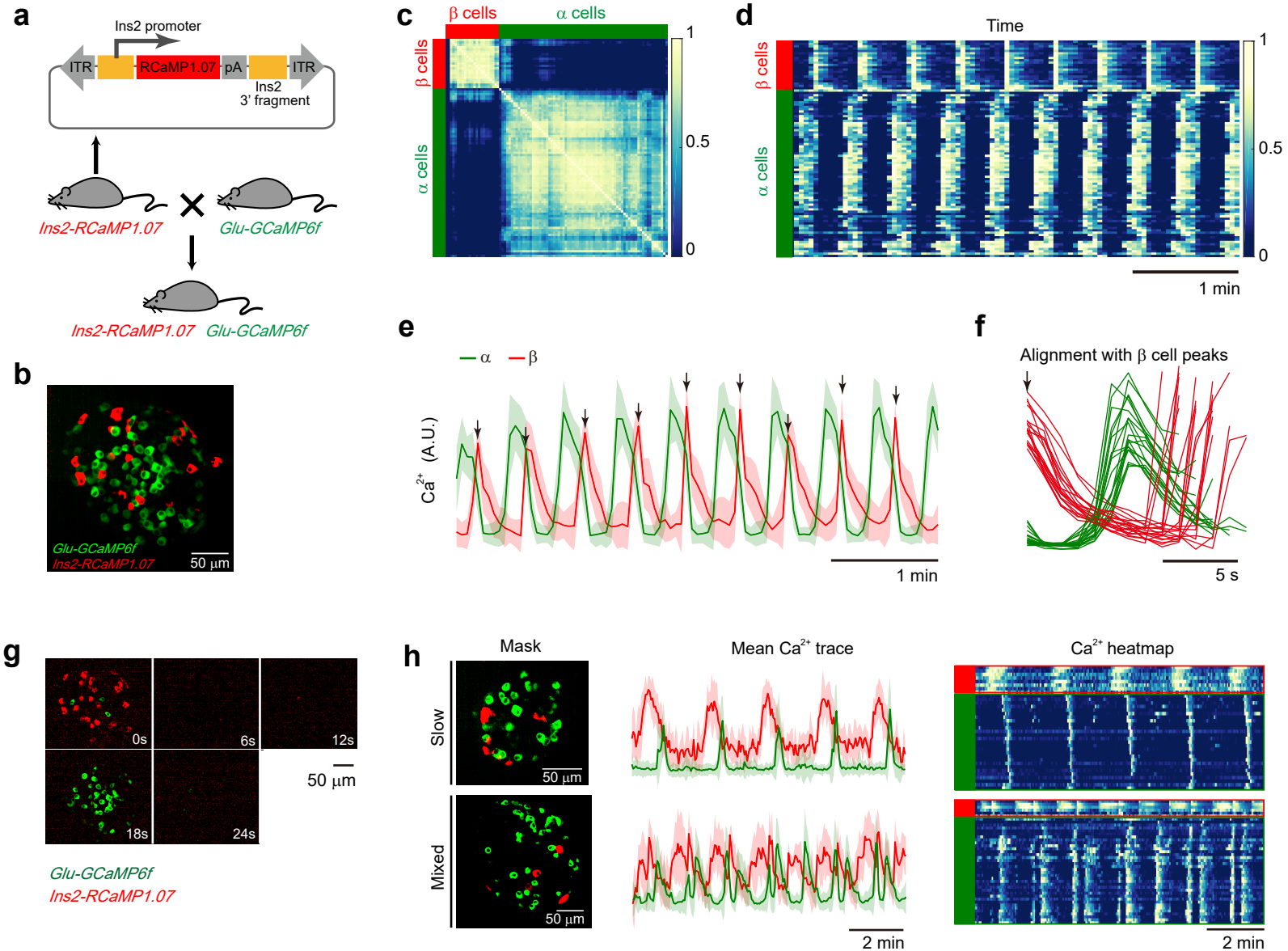

Fig. 2 | α and β cells are globally phase-locked during oscillation

Fig. 2 | α and β cells are globally phase-locked during oscillation

a, Gene targeting vector designed with *Ins2* 5'promoter, *RCaMP1.07* and *Ins2* 3'fragment to construct the *Ins2-RCaMP1.07* mice. By crossbreeding of *Ins2-RCaMP1.07* mice with *Glu-GCaMP6f* mice, we generate the *Glu-GCaMP6f Ins2-RCaMP1.07* mice. **b**, Maximal projection of Ca^{2+} activity from the *Glu-GCaMP6f Ins2-RCaMP1.07* mice islet. α cells express GCaMP6f (Green) and β cells sparsely express RCaMP1.07. **c**, Correlation matrix (Pearson correlation coefficients) for Ca^{2+} activity of islet cells under 10G stimulation. Cells are sorted according to cell types. β cells are indicated by red bar and α cells green bar. α and β cells show strong synchronization within themselves (but not between α and β cells). **d**, Heat-map of Ca^{2+} activity for α and β cells as a function of time under 10G stimulation. Each line represents one cell. α and β cells are global phase-locked during oscillation. **e**, Mean Ca^{2+} activity of α and β cells under 10G stimulation. Shadow indicates standard deviation of each type of cells. The red trace represents β cells and green trace α cells (n=22 for β cells and n=71 for α cells). **f**, Mean Ca^{2+} activity of α and β cells in C, aligned at each β cell peak. Each trace starts from a peak of β cell oscillation and stops in the following peak. **g**, The α and β cells' activation sequence under 10G stimulation. We subtract the previous frame from the next frame of the original Ca^{2+} images and average across oscillations (each oscillation is aligned with the maximum activation frame). The mean activation sequence uses 5 min Ca^{2+} images (frame interval is 3 s). The β cells are colored red and α cells green. **h**, Representative recordings of slow and mixed oscillations of Ca^{2+} activity of α and β cells under 10G stimulation. Top: slow oscillation; bottom: mixed oscillation. First column, maximal projection of Ca^{2+} masks (α cells green and β cells red); second column, mean Ca^{2+} trace of α and β cells (shadow indicates standard deviation); third column, heat-map of α and β cells' Ca^{2+} activity.

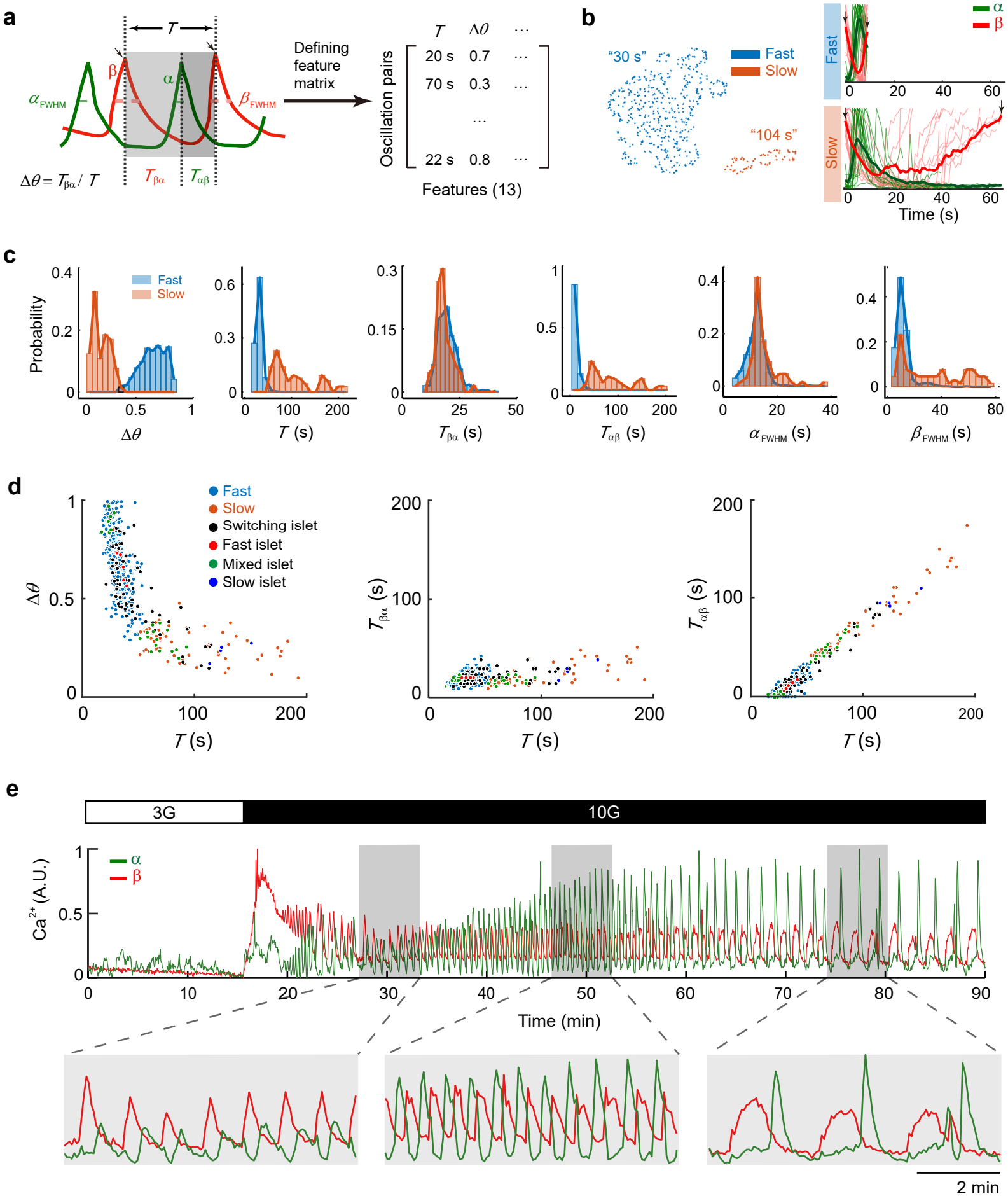

Fig. 3 | α cell activates after β cell with a fixed time delay while β cell activates after α cell with variable time delay

Fig. 3 | α cell activates after β cell with a fixed time delay while β cell activates after α cell with variable time delay

a, Left: each oscillation cycle is defined as the interval between two β cell activations (see Extended Data Fig. 3 for alternative ways to define the period *T*). Right: 13 features of α-β oscillation cycle are used to construct the feature matrix (columns represent features, rows represent oscillation cycles (n=658 cycles from 21 islets)). **b**, Left: oscillation cycles are separated into two clusters by using UMAP (see Supplementary Information), with the mean oscillation period (*T*) of each cluster shown. Right: mean Ca^{2+} traces (bold line) and 15 representative traces (thin line) of fast cluster (top panel) and slow cluster (bottom panel), aligned at the peaks of β cell Ca^{2+} activity (arrows). **c**, Histogram of phase difference ($\Delta\theta$), oscillation period (*T*), waiting time of α and β cells ($T_{\beta\alpha}$ and $T_{\alpha\beta}$), and Full Width at Half Maximum of α and β cells (α_{FWHM}, β_{FWHM}) in fast and slow clusters defined in (**b**). **d**, Top: Scatter plot of $\Delta\theta$ versus period *T* showing an inverse proportional relationship. Middle: $T_{\beta\alpha}$ is independent of *T*. Bottom: $T_{\alpha\beta}$ is linearly dependent on *T*. These relationships hold for various oscillation modes as indicated by the different colors. The blue and orange dots represent the fast and slow clusters in (**b**), respectively. The black dots represent the oscillations from the islet shown in (**e**). The red, green and dark blue dots represent the oscillations from fast, mixed and slow islets in Fig. 4d (right panels). (See Extended Data Fig. 4 for scatter plots of other ways to define the period). **e**, Mean Ca^{2+} traces of α and β cells under 3G (15min) and 10G (75min) stimulation. The oscillation modes change from fast to slow during the long-time 10G stimulation. Note that $\Delta\theta$, *T*, $T_{\alpha\beta}$ and $T_{\beta\alpha}$ here follow the same relationships in (**d**), regardless of oscillation mode change. Three zoomed windows are shown below.

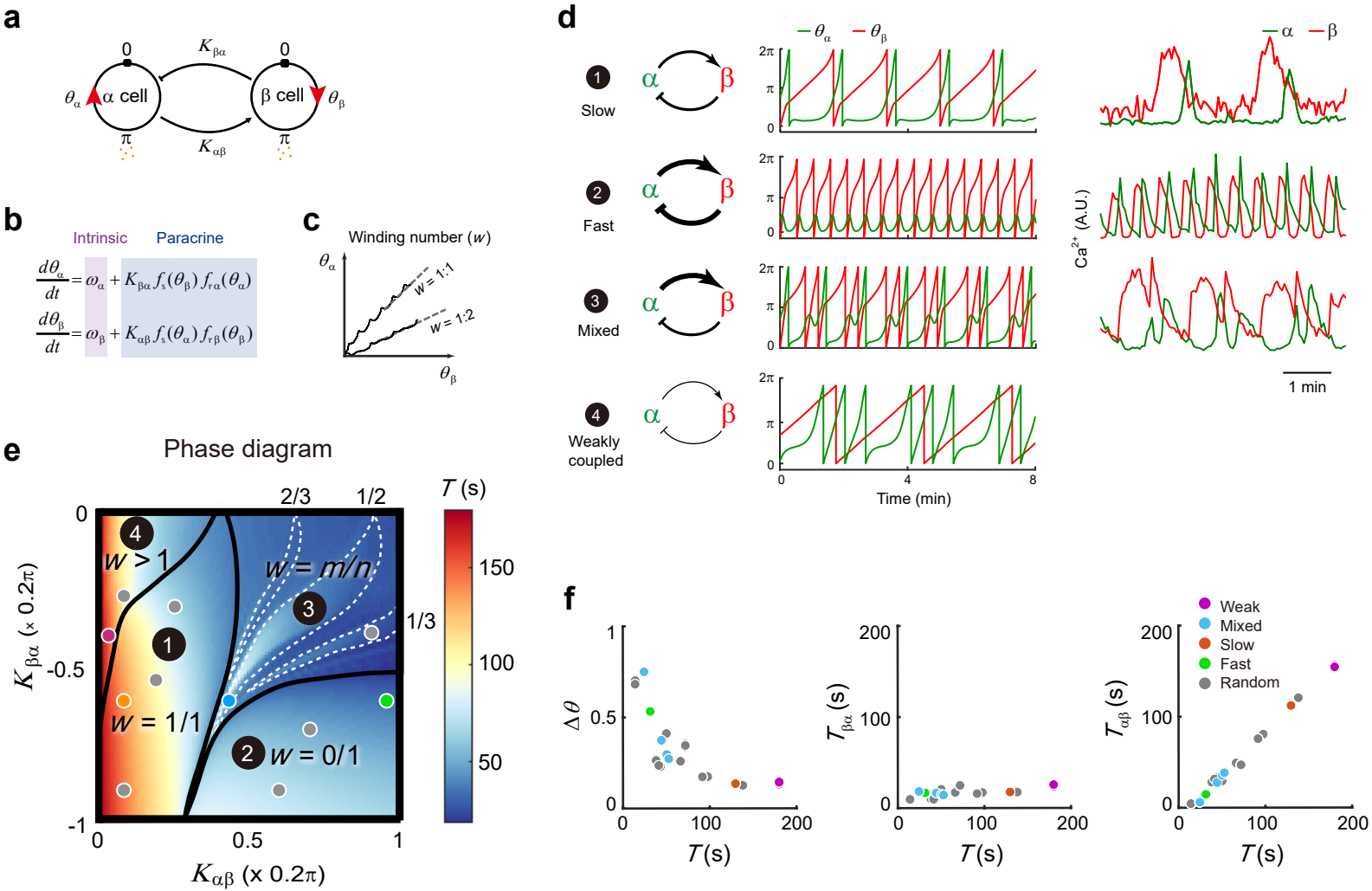

Fig. 4 | Mathematical model of islet α cell and β cell

Fig. 4 | Mathematical model of islet α and β cells

a, Two-cell islet model. The state of each cell is described by its phase θ. Cell secretes hormone at phase π. The hormone secreted by α cell stimulates β cell (with strength $K_{\alpha\beta}$), and the effect of β cell activation inhibits α cell (with strength $K_{\beta\alpha}$). **b**, Equations for phase dynamics of α and β cells. The phase of each cell is influenced by its own intrinsic frequency and the paracrine stimulation/inhibition. Function $f_s(\theta)$ describes the hormone secretion and function $f_r(\theta)$ describes the cell's response to the hormone. **c,** Illustration of winding number (w) definition. Two examples are shown. Solid lines are the actual trajectories of two solutions of the equations in (**b**), and dotted lines are straight lines representing the asymptotic limits of the trajectories that define the winding number. **d**, Left panel: schematic of α and β cells' interaction strengths. Four cases from the four regions in (**e**) are shown. Middle panel: example traces of θ_α and θ_β in the four cases, respectively. The parameters used in these examples are indicated by the four color dots in (**e**). Right panel: corresponding examples of Ca^{2+} traces found experimentally for the first three cases. **e**, The phase diagram of the system. Depending on the two coupling constants $K_{\alpha\beta}$ and $K_{\beta\alpha}$, the oscillatory behavior of the two cells falls into one of the four phase-locked regions, characterized by the winding number w. In region 3, any rational winding number $w<1$ has a stable phase locking region. For clarity, only the phase-locking regions for lower order rational numbers (1/3, 1/2 and 2/3) are shown. Color bar codes the period of the oscillation. **f**, Scatter plots of $\Delta\theta$, $T_{\beta\alpha}$ and $T_{\alpha\beta}$ *versus* T. Each dot represents one oscillation cycle. The color of the dot indicates the parameters used in the simulation, which are shown in the phase diagram (**e**) with the same color.

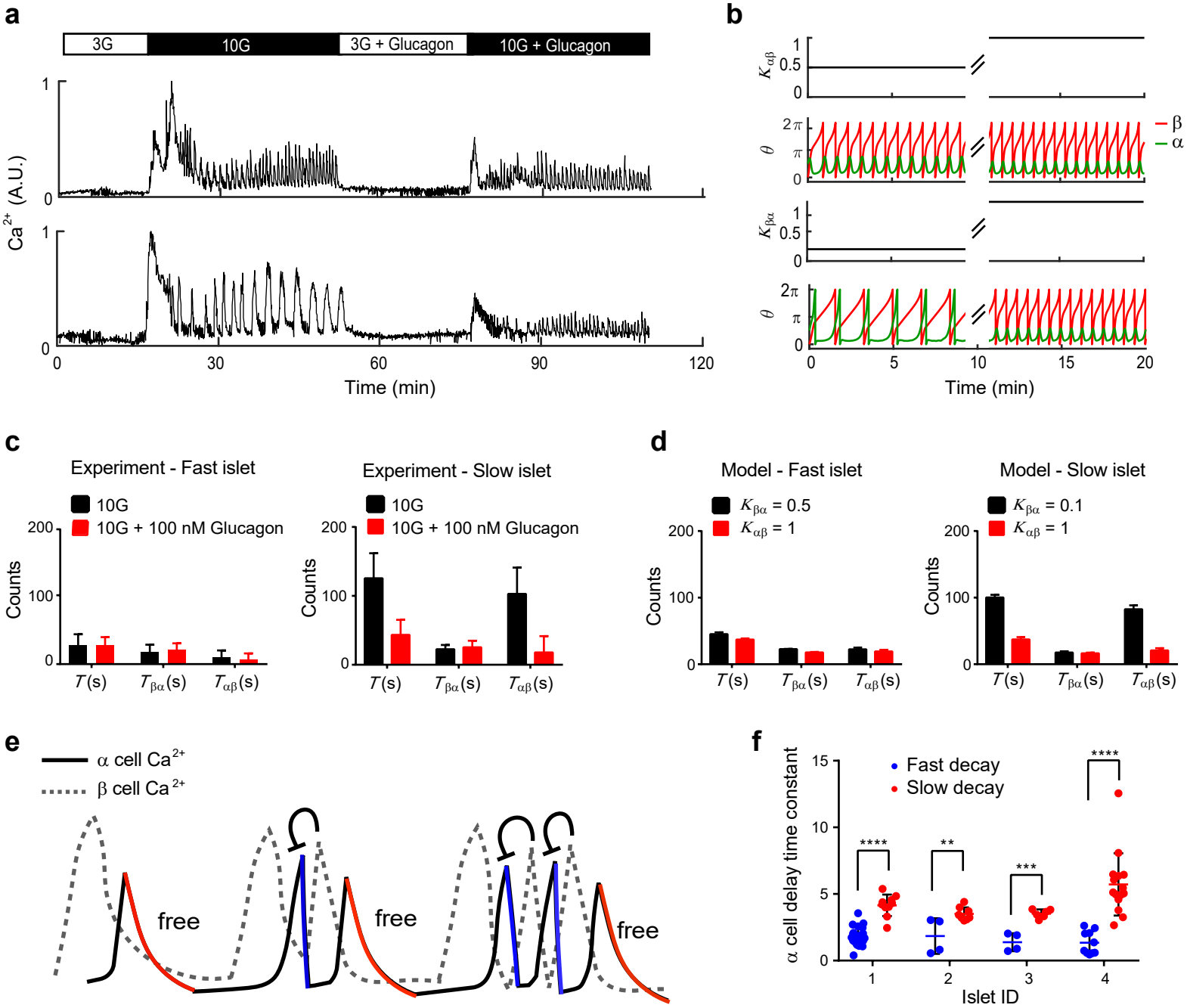

Fig. 5 | Model prediction and experimental verification

Fig. 5 | Model prediction and experimental verification

a, Representative recordings of Ca^{2+} in dual-color labelled transgenic mice for fast (top) and slow (bottom) oscillation islets (only β signal shown here. See Extended Data Fig. 9 for more examples and for both α and β signals). The stimulation used in the experiment is shown above: 3G (15 min), 10G (40 min), 3G+100nM glucagon (30 min) and 10G+100nM glucagon (40 min). **b**, Modeling results for increasing $K_{\alpha\beta}$ on fast (top) and slow (bottom) oscillation islets. Top: Oscillation period remains the same with increasing $K_{\alpha\beta}$. Bottom: Oscillation period becomes shorter with increasing $K_{\alpha\beta}$. **c**, Histogram of T, $T_{\beta\alpha}$ and $T_{\alpha\beta}$ from experiments under 10G stimulation with and without glucagon treatment. Left: fast oscillation islets (n=4 islets). Right: slow oscillation islets (n=3 islets). Values represent mean ± SEM. **d**, Histogram of T, $T_{\beta\alpha}$ and $T_{\alpha\beta}$ from the model. Left: fast oscillation islet from the top of (**b**). Right: slow oscillation islet from the bottom of (**b**). Values represent mean ± SEM. **e**, Schematic of Ca^{2+} traces in islet of mix oscillations. Solid line shows α cell Ca^{2+} activity and dashed line β cell. The α cell transients immediately preceding a β cell activation decay faster (colored red) due to the repression of β cells. The α cell transients away from β cell activation would decay with their own intrinsic dynamics and thus slower (colored blue). **f**, Histograms of the decay time constants (see Extended Data Fig. 3 for the definition) for the two kinds of α cell transients described in (**e**) in mixed oscillations. They clearly fall into two groups: fast (red) and slow (blue). Data from 4 islets are shown. Their Ca^{2+} traces are shown in Extended Data Fig. 10. Values represent mean ± SEM. n.s. $p>0.1$, *$p<0.05$, **$p<0.01$, ***$p<0.001$, ****$p<0.0001$. Two–tailed unpaired Welch's *t*-test.

	Fast cluster	Slow cluster	p^r-value[a]	Significance[b]
T	29.8	99.9	3E-20	****
$\Delta\theta$	0.67	0.24	5E-111	****
$T_{\beta\alpha}$	19.9	17.7	1.7	n.s.
$T_{\alpha\beta}$	9.5	81.2	2E-21	****
α_{FWHM}	11.9	14.8	0.08	n.s.
β_{FWHM}	11.4	31.1	8E-8	****
$\frac{\alpha_{FWHM}}{\beta_{FWHM}}$	1.04	0.48	4E-4	***
τ_{α_up}	5.1	5.0	7E-5	n.s.
τ_{α_decay}	8,8	13.6	8E-7	****
τ_{β_up}	5.1	18.7	7E-5	****
τ_{β_decay}	10.4	20.4	2E-5	****

Table 1 | The mean value of the features in the fast and slow clusters.

[a]Statistical comparisons are conducted using unpaired t test with Welch's correction in Prism 7 (GraphPad Software, La Jolla, CA). Absolute values of p-value are given by TTEST function in Excel(Microsoft, Redmond, WA). Revised p value: $p^r = p(\times 1E5)$. [b]*p^r <0.05, **p^r <0.01, ***p^r <0.001, ****p^r <0.0001. Red labeled features show no significant difference.

Data availability

The data that support the findings of this study and the MATLAB codes are available from the corresponding authors upon request.

Acknowledgements

We thank Erik Gylfe, Anders Tengholm, Yanmei Liu, Louis Tao and Alexander Valentin Nielsen for helpful discussions. We thank Chunxiong Luo and Shujing Wang for help with the microfluidic chip design. We thank Daniel Tang and Iain Bruce for manuscript editing. We thank Yanrong Li for housing mice. This work was supported by grants from the Chinese Ministry of Science and Technology (2015CB910300), National Natural Science Foundation of China (81925022), The National Key Research and Development Program of China (SQ2016YFJC040028, 2018YFA0900700), and NSFC Innovation group projects (31821091).

Author contributions

C.T. and L.C. conceived and supervised the study, and wrote the manuscript.
H.R. led the project, designed experiments, carried out data analysis and mathematical modeling, and wrote the manuscript.
Y.L. designed and manufactured the microfluidic chip, designed and performed experiments, and wrote the manuscript.
C.H. designed and performed experiments, and wrote the manuscript.
X.Y. contributed to figure preparation and supervised experiments, Y.Y and K.S. contributed to the mathematical modeling, B.S. and S.W. contributed to data analysis, X.P., W.Z. and G.Y. contributed to mouse resources.

Competing interests

The authors have no competing financial interests to declare.

Additional information

Supplementary information is available.

References

1. Butler, P. Pulsatile Insulin Secretion Dictates Systemic Insulin Delivery by Regulating Hepatic Insulin Extraction In Humans. *Diabetes* **227**, 190–205 (2005).
2. Matveyenko, A. V., Veldhuis, J. D. & Butler, P. C. Adaptations in pulsatile insulin secretion, hepatic insulin clearance, and β-cell mass to age-related insulin resistance in rats. *Am. J. Physiol. - Endocrinol. Metab.* **295**, (2008).
3. Matveyenko, A. V. *et al.* Pulsatile portal vein insulin delivery enhances hepatic insulin action and signaling. *Diabetes* **61**, 2269–2279 (2012).
4. Stagner, J. I., Samols, E. & Weir, G. C. Sustained oscillations of insulin, glucagon, and somatostatin from the isolated canine pancreas during exposure to a constant glucose concentration. *J. Clin. Invest.* **65**, 939–942 (1980).
5. Hellman, B., Salehi, A., Gylfe, E., Dansk, H. & Grapengiesser, E. Glucose generates coincident insulin and somatostatin pulses and antisynchronous glucagon pulses from human pancreatic islets. *Endocrinology* **150**, 5334–5340 (2009).
6. Lang, D. A., Matthews, D. R., Burnett, M., Ward, G. M. & Turner, R. C. Pulsatile, synchronous basal insulin and glucagon secretion in man. *Diabetes* **31**, 22–26 (1982).
7. Goodner, C. J. *et al.* Insulin, glucagon, and glucose exhibit synchronous, sustained oscillations in fasting monkeys. *Science* **195**, 177–179 (1977).
8. Lang, D. A., Matthews, D. R., Burnett, M. & Turner, R. C. Brief, irregular oscillations of basal plasma insulin and glucose concentrations in diabetic man. *Diabetes* (1981) doi:10.2337/diab.30.5.435.
9. Hansen, B. C., Jen, K. C., Belbez Pek, S. & Wolfe, R. A. Rapid oscillations in plasma insulin, glucagon, and glucose in obese and normal weight humans. *J. Clin. Endocrinol. Metab.* **54**, 785–792 (1982).
10. Rohrer, S. *et al.* Impaired crosstalk between pulsatile insulin and glucagon secretion in prediabetic individuals. *J. Clin. Endocrinol. Metab.* **97**, (2012).
11. Corbin, K. L., Waters, C. D., Shaffer, B. K., Verrilli, G. M. & Nunemaker, C. S. Islet hypersensitivity to glucose is associated with disrupted oscillations and increased impact of proinflammatory cytokines in islets from diabetes-prone male mice. *Endocrinology* **157**, 1826–1838 (2016).
12. Valdeolmillos, M., Santos, R. M., Contreras, D., Soria, B. & Rosario, L. M. Glucose-induced oscillations of intracellular Ca2+ concentration resembling bursting electrical activity in single mouse islets of Langerhans. *FEBS Lett.* (1989) doi:10.1016/0014-5793(89)81484-X.
13. Liu, Y. J., Tengholm, A., Grapengiesser, E., Hellman, B. & Gylfe, E. Origin of slow and fast oscillations of Ca2+ in mouse pancreatic islets. *J. Physiol.* (1998) doi:10.1111/j.1469-7793.1998.471bq.x.
14. Zhang, M., Goforth, P., Bertram, R., Sherman, A. & Satin, L. The Ca2+ dynamics of isolated mouse β-cells and islets: Implications for mathematical models. *Biophys. J.* **84**, 2852–2870 (2003).
15. Chay, T. R. & Keizer, J. Minimal model for membrane oscillations in the pancreatic beta-cell. *Biophys. J.* **42**, 181–189 (1983).
16. Bertram, R., Satin, L. S. & Sherman, A. S. Closing in on the mechanisms of pulsatile insulin secretion. *Diabetes* **67**, 351–359 (2018).
17. Wierschem, K. & Bertram, R. Complex bursting in pancreatic islets: A potential glycolytic mechanism. *J. Theor. Biol.* (2004) doi:10.1016/j.jtbi.2004.02.022.
18. Zimliki, C. L., Mears, D. & Sherman, A. Three roads to islet bursting: Emergent oscillations in coupled phantom bursters. *Biophys. J.* **87**, 193–206 (2004).
19. Dryselius, S., Grapengiesser, E., Hellman, B. & Gylfe, E. Voltage-dependent entry and generation of slow Ca2+ oscillations in glucose-stimulated pancreatic β-cells. *Am. J. Physiol. - Endocrinol. Metab.* (1999) doi:10.1152/ajpendo.1999.276.3.e512.
20. Hellman, B., Gylfe, E., Grapengiesser, E., Lund, P. E. & Berts, A. Cytoplasmic Ca2+ oscillations in pancreatic ß-cells. *BBA - Reviews on Biomembranes* (1992) doi:10.1016/0304-4157(92)90003-S.
21. Gilon, P., Jonas, J. C. & Henquin, J. C. Culture duration and conditions affect the oscillations of cytoplasmic calcium concentration induced by glucose in mouse pancreatic islets. *Diabetologia* (1994) doi:10.1007/BF00400464.
22. Tengholm, A. & Gylfe, E. Oscillatory control of insulin secretion. *Mol. Cell. Endocrinol.* **297**, 58–72 (2009).

23. Li, J. *et al.* Submembrane ATP and Ca2+ kinetics in α-cells: Unexpected signaling for glucagon secretion. *FASEB J.* **29**, 3379–3388 (2015).
24. Hellman, B., Salehi, A., Grapengiesser, E. & Gylfe, E. Isolated mouse islets respond to glucose with an initial peak of glucagon release followed by pulses of insulin and somatostatin in antisynchrony with glucagon. *Biochem. Biophys. Res. Commun.* **417**, 1219–1223 (2012).
25. Meier, J. J., Kjems, L. L., Veldhuis, J. D., Lefèbvre, P. & Butler, P. C. Postprandial suppression of glucagon secretion depends on intact pulsatile insulin secretion: Further evidence for the intraislet insulin hypothesis. *Diabetes* **55**, 1051–1056 (2006).
26. Menge, B. A. *et al.* Loss of inverse relationship between pulsatile insulin and glucagon secretion in patients with type 2 diabetes. *Diabetes* **60**, 2160–2168 (2011).
27. Capozzi, M. E. *et al.* β Cell tone is defined by proglucagon peptides through cAMP signaling. *JCI insight* **4**, (2019).
28. Svendsen, B. *et al.* Insulin Secretion Depends on Intra-islet Glucagon Insulin Secretion Depends on Intra-islet Glucagon Signaling. *CellReports* **25**, 1127-1134.e2 (2018).
29. Franklin, I., Gromada, J., Gjinovci, A., Theander, S. & Wollheim, C. B. b-Cell Secretory Products Activate a-Cell ATP-Dependent Potassium Channels to Inhibit Glucagon Release. **54**, (2005).
30. Gylfe, E. & Tengholm, A. Neurotransmitter control of islet hormone pulsatility. *Diabetes, Obes. Metab.* **16**, 102–110 (2014).
31. Watts, M., Ha, J., Kimchi, O. & Sherman, A. Paracrine regulation of glucagon secretion: The β/α/δ model. *Am. J. Physiol. - Endocrinol. Metab.* **310**, E597–E611 (2016).
32. Hoang, D. T., Hara, M. & Jo, J. Design principles of pancreatic islets: Glucose-dependent coordination of hormone pulses. *PLoS One* **11**, 1–17 (2016).
33. Merkwitz, C. *et al.* The ductal origin of structural and functional heterogeneity between pancreatic islets. *Prog. Histochem. Cytochem.* **48**, 103–140 (2013).
34. Dybala, M. P. & Hara, M. Heterogeneity of the human pancreatic islet. *Diabetes* **68**, 1230–1239 (2019).
35. Ravier, M. a *et al.* Loss of Connexin36 channels alters beta cell coupling islet synchronization of glucose insduced ca and insulin oscillations and basal insulin release. *Diabetes* **54**, 1798–1807 (2005).
36. Benninger, R. K. P. *et al.* Intrinsic islet heterogeneity and gap junction coupling determine spatiotemporal Ca2+wave dynamics. *Biophys. J.* **107**, 2723–2733 (2015).
37. Calabrese, A. *et al.* Connexin 36 controls synchronization of Ca2+oscillations and insulin secretion in MIN6 cells. *Diabetes* **52**, 417–424 (2003).
38. Benninger, R. K. P., Zhang, M., Steven Head, W., Satin, L. S. & Piston, D. W. Gap junction coupling and calcium waves in the pancreatic islet. *Biophys. J.* **95**, 5048–5061 (2008).
39. Qiu, W. L. *et al.* Deciphering Pancreatic Islet β Cell and α Cell Maturation Pathways and Characteristic Features at the Single-Cell Level. *Cell Metab.* **25**, 1194-1205.e4 (2017).
40. Mcinnes, L., Healy, J. & Melville, J. UMAP : Uniform Manifold Approximation and Projection for Dimension Reduction arXiv : 1802 . 03426v2 [stat . ML] 6 Dec 2018. (2018).
41. Kudrewicz, J. & Wasowicz, S. *Equations of Phase-Locked Loops, Dynamics on the Circle, Torus and Cylinder*. (Singapore: World Scientific Publishing, 2007).
42. Rorsman, P. & Huising, M. O. The somatostatin-secreting pancreatic δ-cell in health and disease. *Nature Reviews Endocrinology* (2018) doi:10.1038/s41574-018-0020-6.
43. Briant, L. J. B. *et al.* Δ-Cells and B-Cells Are Electrically Coupled and Regulate A-Cell Activity Via Somatostatin. *J. Physiol.* **596**, 197–215 (2018).
44. Henquin, J. C., Meissner, H. P. & Schmeer, W. Cyclic variations of glucose-induced electrical activity in pancreatic B cells. *Pflügers Arch. Eur. J. Physiol.* **393**, 322–327 (1982).
45. Sánchez-Andrés, J. V., Gomis, A. & Valdeolmillos, M. The electrical activity of mouse pancreatic beta-cells recorded in vivo shows glucose-dependent oscillations. *J. Physiol.* **486**, 223–228 (1995).
46. Fernandez, J. & Valdeolmillos, M. Synchronous glucose-dependent [Ca2+](i) oscillations in mouse pancreatic islets of Langerhans recorded in vivo. *FEBS Lett.* (2000) doi:10.1016/S0014-5793(00)01631-8.
47. Salem, V. *et al.* Leader β-cells coordinate Ca2+ dynamics across pancreatic islets in vivo. *Nat. Metab.* **1**, 615–629 (2019).